



One-step synthesis of magnetic chitosan for controlled release of 5-hydroxytryptophan



Jucely dos Santos Menegucci, Mac-Kedson Medeiros Salviano Santos, Diego Juscelino Santos Dias, Juliano Alexandre Chaker, Marcelo Henrique Sousa*

Universidade de Brasília, Faculdade de Ceilândia, Centro Metropolitano Cj. A Lt. 1, Ceilândia – DF CEP 72220-900, Brazil

ARTICLE INFO

Article history:

Received 21 June 2014

Received in revised form

30 September 2014

Accepted 4 October 2014

Available online 12 October 2014

Keywords:

Magnetic nanoparticles

Chitosan

Nanocomposite

Controlled release

5-Hydroxytryptophan

ABSTRACT

In this work, nanoparticles of chitosan embedded with 25% (w/w) of iron oxide magnetic nanoparticles (magnetite/maghemite) with narrow size-distribution and with a loading efficiency of about 80% for 5-hydroxytryptophan (5-HTP), which is a chemical precursor in the biosynthesis of important neurotransmitters as serotonin, were synthesized with an initial mass ratio of 5-HTP/magnetic chitosan=1.2, using homogeneous precipitation by urea decomposition, in an efficient one-step procedure. Characterization of morphology, structure and surface were performed by XRD, TEM, FTIR, TGA, magnetization and zeta potential measurements, while drug loading and drug releasing were investigated using UV–vis spectroscopy. Kinetic drug release experiments under different pH conditions revealed a pH-sensitive controlled-release system, ruled by polymer swelling and/or particle dissolution.

© 2014 Elsevier B.V. All rights reserved.

1. Introduction

Design and tailoring of controlled release (CR) systems have been extensively studied, in order to enhance drug therapy and increase patient compliance. This has become possible because CR systems can control drug exposure over time, help drugs to pass through physiological barriers, protect drugs from premature elimination, drive drugs to the target site, minimize drug exposure and reduce frequency of administration [1]. For these purposes, various biodegradable polymers have been used in drug delivery research; they can effectively deliver the drug to a target site and thus increase the therapeutic benefit, while minimizing side effects [2]. One of these biopolymers which has attracted attention in the controlled release field is chitosan (CS), a natural polysaccharide that presents low toxicity, improved mucoadhesive features and antimicrobial properties. From the chemical point of view, CS presents amine (NH₂) and hydroxyl (OH) groups that are readily available for crosslinking with drugs or biological entities [3].

Chitosan can be combined with magnetic materials which are highly useful in the development of novel stimuli-responsive materials for drug delivery – the presence of magnetic materials gives advantages such as detectability by imaging techniques, controllability by an external magnetic field and thermal heating

which has been used to produce tissue ablation or to control drug release [4]. Magnetic nanoparticles (MNPs) are also widely appreciated in biomedical applications [5] because they present high surface area to volume ratio, facility to be conjugated with biomolecules and manipulability by an external magnetic field – they also present lower sedimentation rates and improved tissue diffusion [6]. However, due to their chemical nature, MNPs – normally iron oxides – are non-biocompatible and need to be functionalized before biomedical applications. This can be achieved by encapsulating or dispersing them into a biocompatible polymeric matrix [7]. Thus, the combination of MNPs with CS would enhance both materials' characteristics for new applications. In fact, there are several reports of chitosan conjugated with magnetic nanoparticles for different purposes which range from magnetic adsorbents in environmental applications [8] to controlled drug delivery/release [9] and magnetic hyperthermia in the biomedical field [10].

Despite its potential, magnetic chitosan as a vehicle for drug release has not been widely explored yet. Moreover, simple and reproducible approaches to fabricate CR systems with magnetic-responsive properties that can provide efficient drug loading, controllable drug release, and imaging capability are highly desirable. In this work we propose a simple fabrication of a nanocomposite which consists of chitosan structures embedded with magnetic iron oxide nanoparticles as a magnetic-responsive system for the controllable release of drugs. The novelty of this work is that the synthesis route is environmentally friendly and

* Corresponding author.

E-mail address: mhsqui@gmail.com (M.H. Sousa).

comprises combination of the composite and drug in only one step. Here, 5-hydroxytryptophan (5-HTP) – which is a chemical precursor in the biosynthesis of important neurotransmitters as serotonin [11] – was chosen for drug loading since it has a great affinity for chitosan; additionally, because it is easily monitored spectrophotometrically, 5-HTP was used as a surrogate small, water-soluble drug.

Thus, using a method of homogeneous precipitation by urea decomposition, efficient one-pot synthesis of a nanocomposite comprising large aggregates of CS nanoparticles embedded with about 25% (w/w) of magnetic nanoparticles and with a loading efficiency of about 80% for an initial mass ratio of 5-HTP/magnetic chitosan=1.2, could be achieved. Moreover, kinetic drug release experiments under different pH conditions revealed that this is a pH-sensitive controlled-release system and that drug release is more efficient in an acidic medium.

2. Experimental section

All the chemical reagents used in the work were of analytical grade and were used without further purification.

2.1. Magnetic chitosan (mag@CS)

In a typical procedure, for the synthesis of magnetic chitosan, 1.0 mL of 1% (w/w) chitosan solution (high purity, Mv 60,000–120,000, from Sigma-Aldrich) – prepared in 1% (w/w) acetic acid – and 40 mmol of urea were dissolved in 50 mL of water at room temperature. Then, 20 μ mol of $\text{FeCl}_3 \cdot 6\text{H}_2\text{O}$ and 10 μ mol of $\text{FeCl}_2 \cdot 4\text{H}_2\text{O}$ were mixed uniformly into the solution containing urea and chitosan, in a three-neck flask, and the temperature was

brought to 100 °C under moderate reflux while stirring, for 4 h. The product was collected and washed several times with water, by magnetic decantation.

2.2. 5-HTP loading

Two methods were utilized for the incorporation of 5-HTP into magnetic chitosan. In the first approach, lyophilized magnetic chitosan, obtained as described in the section before, was incubated into 5-HTP solution (0.5 mg/mL) for 4 h. In the second method, 5-HTP was mixed with chitosan, urea and iron salts and submitted to a reflux as described in the section before. In both methods, the mass ratio of 5-HTP to magnetic chitosan was 1.2. After loading, solid was separated from supernatant, washed once with water and lyophilized.

2.3. 5-HTP release

The release of 5-HTP was investigated at constant temperature (25 °C) using different pH conditions. In a typical procedure, 20 mg of magnetic chitosan loaded with 5-HTP was introduced in 5 mL of water. Then, pH of the slurry was adjusted and aliquots of supernatant (magnetically separated) were investigated by UV–vis.

2.4. Characterization

The size and morphology of the as-prepared materials were examined by high-resolution transmission electron microscopy (HRTEM) using a JEOL 1100 apparatus. X-ray diffraction study was performed on powder samples with a Rigaku-Miniflex 600 diffractometer using radiation of 1.541 Å (40 kV and 30 mA). The room-temperature magnetization curves were obtained using an

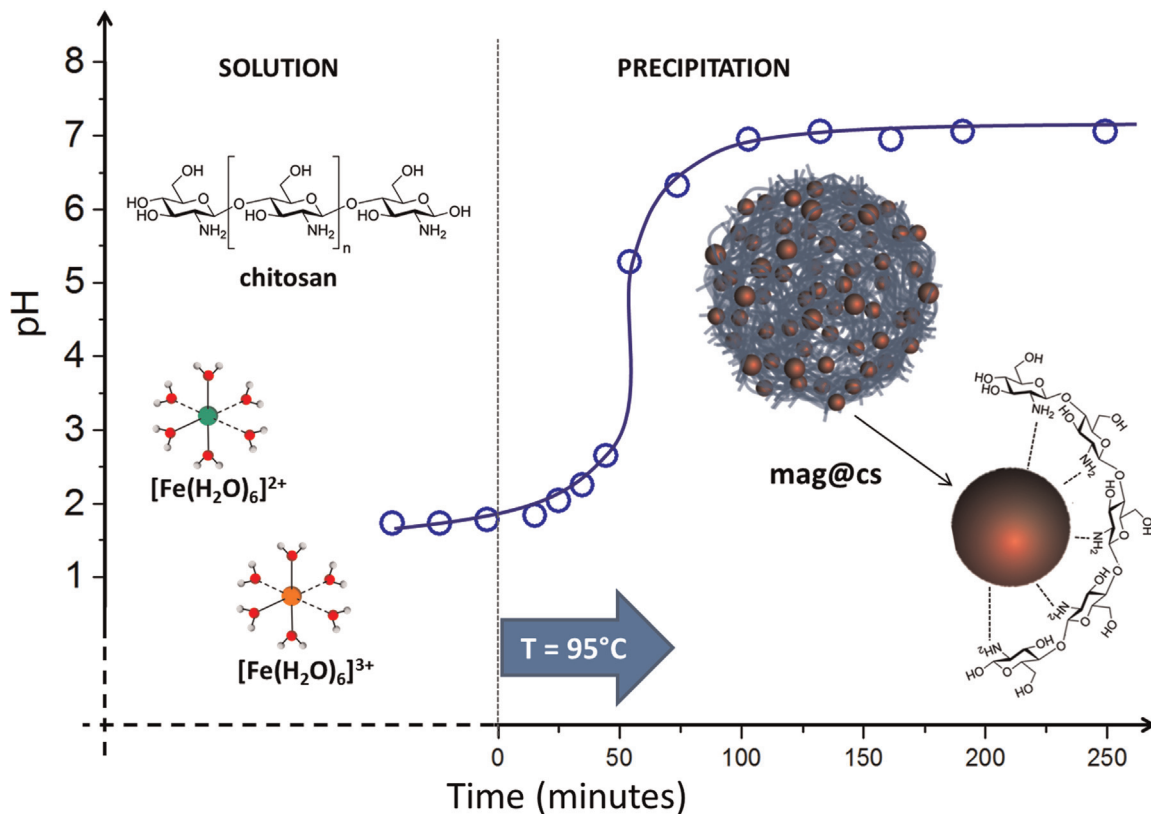
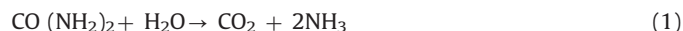


Fig. 1. Schema of synthesis of mag@CS nanocomposites. Circles are the variation of pH as a function of the time of reaction. Before 95 °C, iron complexes and chitosan coexists in the solution. As the temperature reaches 95 °C and time increases, chitosan polymerizes (blue thread ball) embedded with magnetic iron oxide nanoparticles (red spheres). (For interpretation of the references to color in this figure legend, the reader is referred to the web version of this article.)

ADE vibrating sample magnetometer model EV7. Hysteresis loops were performed under applied magnetic fields varying from -18 to 18 kOe at 300 K. A dynamic light scattering analyzer (Malvern Instruments, Zetasizer nano ZS) was used to measure the electrophoretic mobility. FTIR spectra were recorded with crystalline KBr in the range of 3700 – 400 cm^{-1} and resolution of 2 cm^{-1} . Thermogravimetric analyzes (TGA) were performed in air flow and with a heating rate of 10 $^{\circ}\text{C}/\text{min}$ up to 600 $^{\circ}\text{C}$, in a Shimadzu Thermogravimetric Analyzer model DTG-60. The concentration of loaded 5-HTP was measured by determining its concentration in solution, by ultraviolet-visible spectrometry (UV-vis) after and before interaction with magnetic chitosan.

3. Results and discussion

In the synthesis of magnetic chitosan (mag@CS), as temperature reached about 100 $^{\circ}\text{C}$, decomposition of urea takes place and hydroxide concentration increases. In fact, this process generates OH^{-} homogeneously in the solution and, as the urea source is not totally consumed, pH maintains constant at alkaline region [12] as shown in Fig. 1 – the circles represent the pH variation during synthesis. This can be described by reactions (1) and (2).



After about 30 min, a brown gummy colloid started forming and, as time elapsed, this brown precipitate was converted to a black solid. Here, both chitosan and magnetic iron oxide were condensed to form a composite as illustrated in Fig. 1 (the mag@CS structure). Before urea decomposition, the medium was acidic and chitosan was solubilized, but precipitated/coacervated when it came in contact with the alkaline solution originated from reactions (1) and (2) [13]. The presence of Fe^{3+} and Fe^{2+} (aqua ions at acidic pH) at a molar ratio of $2:1$ and the increasing concentration of hydroxide led to the formation of magnetite (Fe_3O_4), according to the chemical reaction $2\text{Fe}^{3+} + \text{Fe}^{2+} + 8\text{OH}^- \rightarrow \text{Fe}_3\text{O}_4 \downarrow + 4\text{H}_2\text{O}$.

XRD pattern of mag@CS sample in Fig. 2 revealed two phases: after indexing the main peaks using Bragg's law and comparing them to the ASTM standards, spinel structure was found, indicating that magnetite and/or maghemite (marked by their indices) should be present in samples synthesized in this work – XRD patterns of magnetite and maghemite are very analogous. When compared with the ASTM lattice parameters for cubic magnetite and maghemite, respectively, 0.8396 nm and 0.8347 nm, the intermediary value of lattice parameter determined for our sample (0.836 nm) indicated that magnetite was partially oxidized to maghemite ($\gamma\text{-Fe}_2\text{O}_3$). This can be explained by the fact that preparations were carried out in air, an oxidizing environment, so that magnetite was partially converted to maghemite [14]. The other phase identified from XRD pattern in Fig. 2 was the chitosan. In fact, the broad peak at $2\theta \sim 20^{\circ}$ is typical of polymerized chitosan [15].

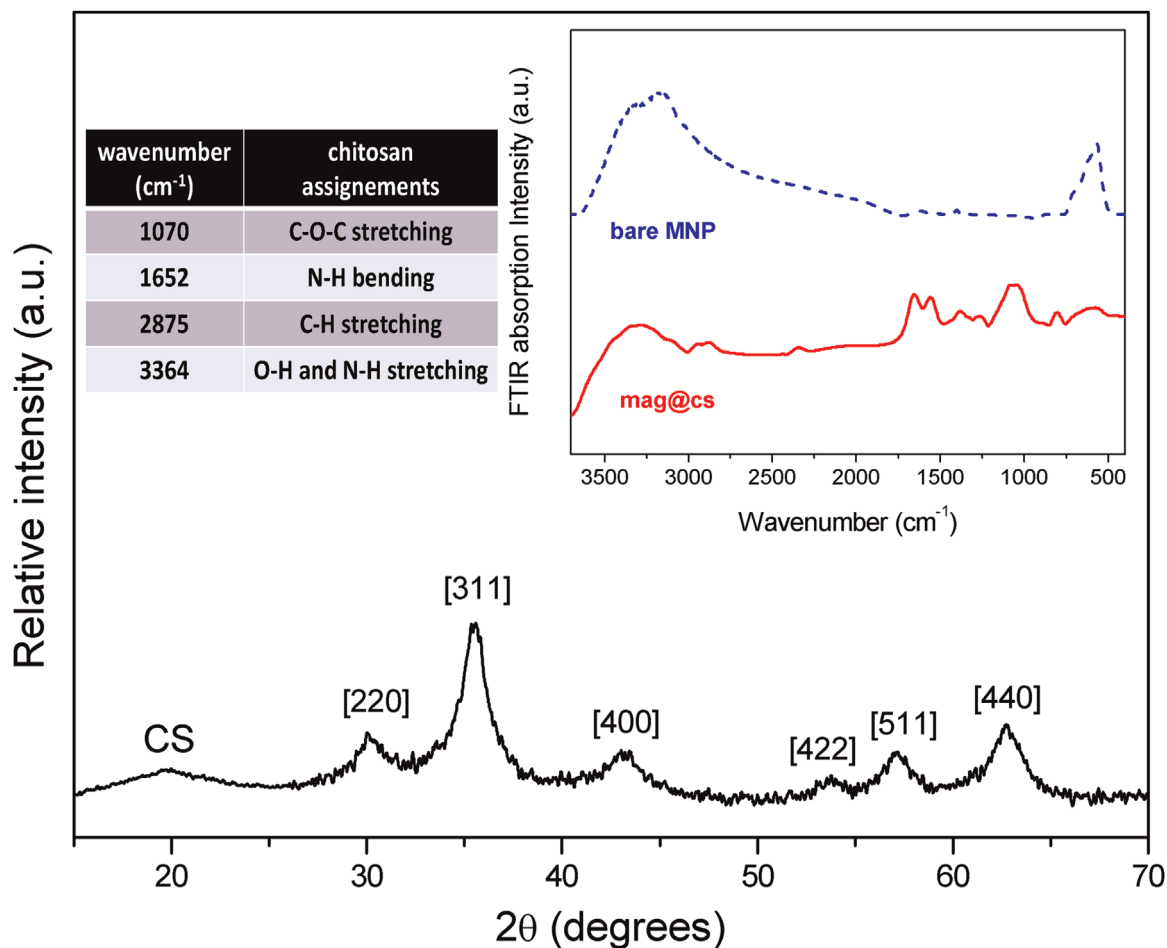


Fig. 2. X-ray diffraction pattern of the mag@CS composite. Main diffraction peaks of iron oxide (magnetite and/or maghemite) are identified by their indices and reflection of chitosan is identified by CS. At the top right corner are the FTIR spectra of bare magnetic nanoparticles (dashed blue) and the mag@CS sample (red). Inset table lists the main FTIR transitions for pure chitosan. (For interpretation of the references to color in this figure legend, the reader is referred to the web version of this article.)

In spite of XRD identifying both the polymeric and inorganic magnetic phases, this technique is not able to prove that they are interacting to form a composite. FTIR was therefore utilized to study the synthesized materials. The insets of Fig. 2 show the FTIR spectra corresponding to the mag@CS composite and to the bare magnetic nanoparticles – the polymer was eliminated after washing the composite with acetic acid and water – and a table with the main infrared transitions observed in the FTIR spectra of pure chitosan. The IR bands around 580 cm^{-1} , attributed to ferrite Fe–O absorptions, as well as the absorption at 3345 cm^{-1} , which is related to OH stretching from oxide surface, are present in both samples [16]. Moreover, since most of the vibrational modes that correspond to pure chitosan – the C–O–C stretching vibrations at 1070 cm^{-1} ; N–H bending at 1652 cm^{-1} ; C–H stretching at 2875 cm^{-1} and O–H and N–H stretching at 3364 cm^{-1} – are shifted to lower wavenumbers and as composites were exhaustively washed after synthesis, FTIR results strongly indicate that chitosan is coordinated to the iron ions on the magnetic nanoparticles via nitrogen groups [17] as illustrated at the bottom right corner of Fig. 1.

From HRTEM analysis it was possible to identify large aggregates of polymeric structures of chitosan with inlaid magnetic iron oxide (magnetite/maghemite) nanoparticles (see Fig. 3). Considering a log-normal distribution, the analysis of magnetic nanoparticles shown in the higher magnification of sample (inset (b)) indicates that homogenous precipitation technique potentially reduces the magnetic nanoparticle size distribution when compared with standard coprecipitation techniques [18]. Indeed, the mean size of magnetic nanoparticles was 7.1 nm and size dispersion 0.16. Further, the lattice fringes ($\sim 0.48\text{ nm}$) observed in the inset (c) agree well with the distance between the (111) lattice planes, common to both iron oxides.

Dynamic light scattering measurements were employed to study the interface of nanocomposites with solution. In this way, samples were dispersed at different pH and the zeta potential was measured. Dependence of zeta potential on the pH, for sample mag@CS, is shown in Fig. 4 (hexagon dots). In acidic medium, nanocomposites are positively charged and, as pH increases, this charge decreases and becomes negative, after passing through zero, at $\text{pH} \sim 8$. This can be understood by taking into account the pH surface dependence characteristics of the chitosan polymer and those of magnetic nanoparticles. For bare MNPs, the dependence of surface charge on the pH is already well known and shows that for extreme pH values, surface charge reaches the maximum, while when close to neutral pH the surface charge is very small. As schematized in Fig. 4, the MNP surface (MNP \blacktriangleright) behaves as a diprotic acid, leading to three kinds of surface sites where most of them are MNP $\blacktriangleright\text{-OH}_2^+$ in strong acidic medium, MNP $\blacktriangleright\text{-O}^-$ in strong basic medium and MNP $\blacktriangleright\text{-OH}$, the intermediate amphoteric sites, in the neutral region [19]. On the other hand, chitosan is a polysaccharide that presents a low electrical charge in neutral and basic pH conditions, but it is positively charged in a more acidic medium [20]. This is due to the fact that free amine groups on the chitosan surface (CS \blacktriangleright) follow the chemical equilibrium $\text{CS } \blacktriangleright\text{-NH}_3^+ + \text{H}_2\text{O} \rightleftharpoons \text{CS } \blacktriangleright\text{-NH}_2 + \text{H}_3\text{O}^+$. Thus, considering that the chitosan particle surface behaves like a monoprotic acid, the molar fraction of CS $\blacktriangleright\text{-NH}_3^+$ will be equal $[\text{H}_3\text{O}^+]/([\text{H}_3\text{O}^+] + K_a^{\text{CS}})$ and the fraction of CS $\blacktriangleright\text{-NH}_2$ will be $K_a^{\text{CS}}/([\text{H}_3\text{O}^+] + K_a^{\text{CS}})$, where K_a^{CS} is the acid dissociation constant of chitosan ($\sim 5 \times 10^{-7}$ [21]). Using this mean value of K_a^{CS} , both molar fractions were also plotted on the graph of Fig. 4 and are shown by red curves. The speciation diagrams for MNPs – i.e. the molar fractions of MNP $\blacktriangleright\text{-OH}_2^+$, MNP $\blacktriangleright\text{-OH}$ and MNP $\blacktriangleright\text{-O}^-$ – are also represented by the blue curves in the graph.

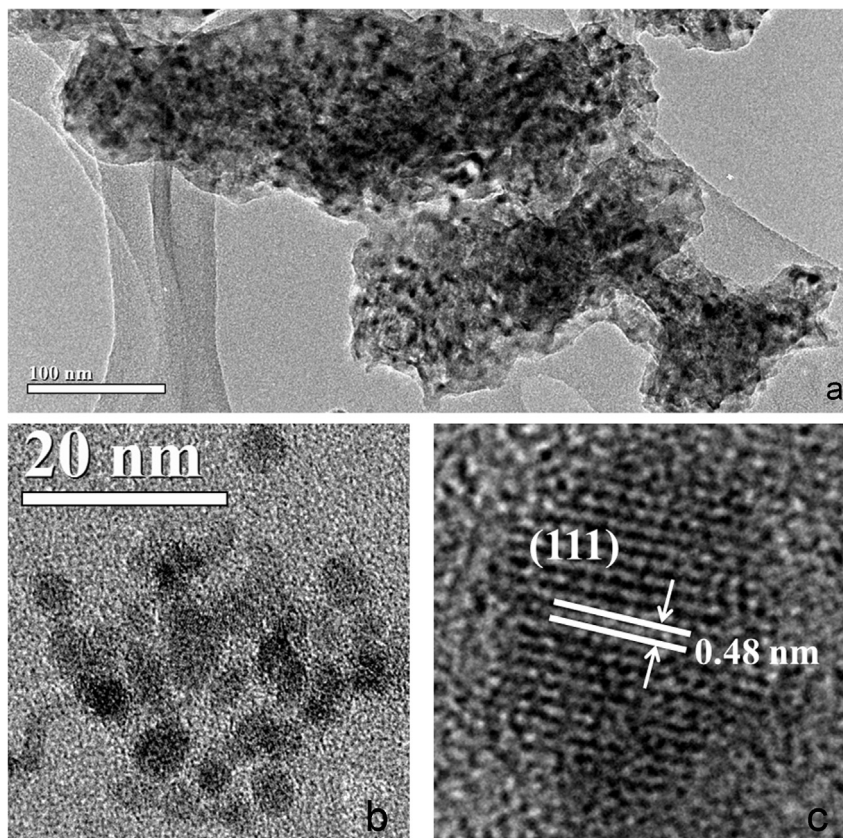


Fig. 3. HRTEM images of the mag@CS composite (a), magnification showing magnetic nanoparticles embedded in the chitosan polymer (b) and lattice fringes of iron oxide (c).

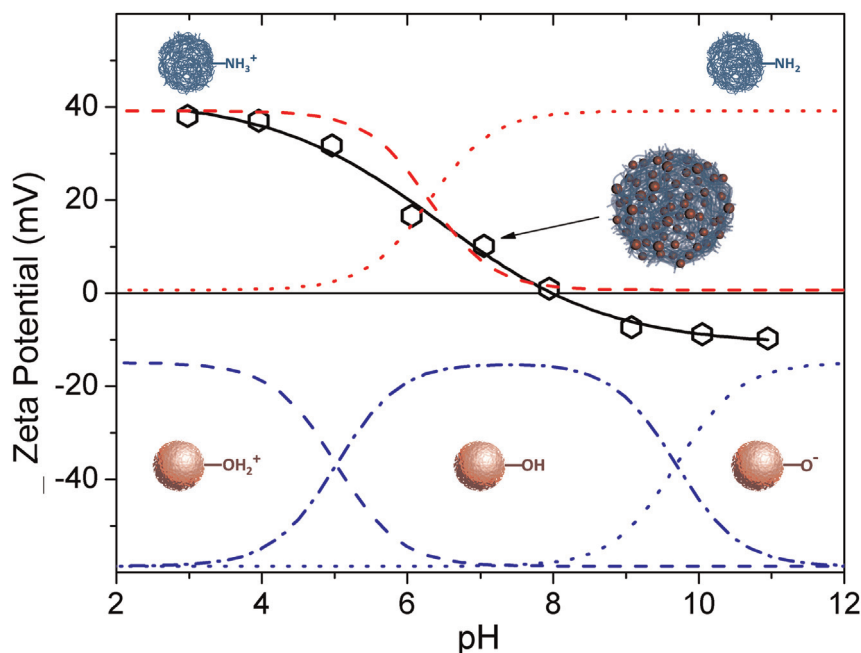


Fig. 4. Zeta potential variation as a function of the pH solution (hexagons) for mag@CS – the black full line is a guide to the eyes. The variation of the molar fraction, as a function of pH, of CS-NH₂ and CS-NH₃⁺ species for pure chitosan is represented by the red dashed and dotted lines, respectively. For magnetic nanoparticles, molar fractions of species MNP-OH₂⁺, MNP-OH and MNP-O⁻ are represented, respectively, by the blue dashed, dot-dashed and dotted lines. (For interpretation of the references to color in this figure, the reader is referred to the web version of this article.)

Thus, it seems that surface features of nanocomposite mag@CS are ruled mainly by the amino-groups of chitosan but are also (less) governed by the surface of iron oxide nanoparticles exposed to the solution. In summary, the positive saturation of charge at lower pH is due to both polymer and MNP protonation. As neutrality is achieved, inorganic and organic phases tend to be discharged. In particular, the low negative charge observed in alkaline medium could be attributed to the MNP-O⁻ species, since chitosan presents no charges (CS-NH₂) at these pHs, or could be due to the formation of the negatively charged species (CS-NH₂OH⁻).

Moreover, taking into account the speciation diagrams shown in Fig. 4, and since synthesis occurs in weak alkaline medium, one infers that interaction of chitosan with MNP is mainly done by the species CS-NH₂ and MNP-OH, through complexation of iron ions on the MNP surface by amino-groups on chitosan, corroborating FTIR observations and, as expected, reflecting the high stability of the iron-amine complexes [22].

For estimation of the mass percentage of MNPs in the nanocomposite, thermogravimetric analysis was used. Thus, most of the loss of mass presented by the mag@CS sample in Fig. 5 is attributed to the thermal decomposition of chitosan, with a first region of loss of mass that occurs at lower temperatures, due to the release of water. For pure chitosan, the maximum weight loss was about 87.5%. The MNPs also presented a loss of mass which mostly originated from free and chemically bonded water. Here, this loss was evaluated at about 4.6% and its TGA curve is presented in the inset of Fig. 5. Bare MNP were obtained after washing the mag@CS sample with acetic acid solution several times, by magnetic decantation. Thus, for estimating the mass percentage of magnetic material on the composite, the losses of mass from pure chitosan and from bare MNPs were subtracted from the loss of mass of mag@CS (41.7%), yielding a magnetic content of 24.6%.

Magnetization measurements were performed for evaluating the counterparts of polymeric coating and magnetic iron oxide nanoparticles on the magnetic properties of the synthesized

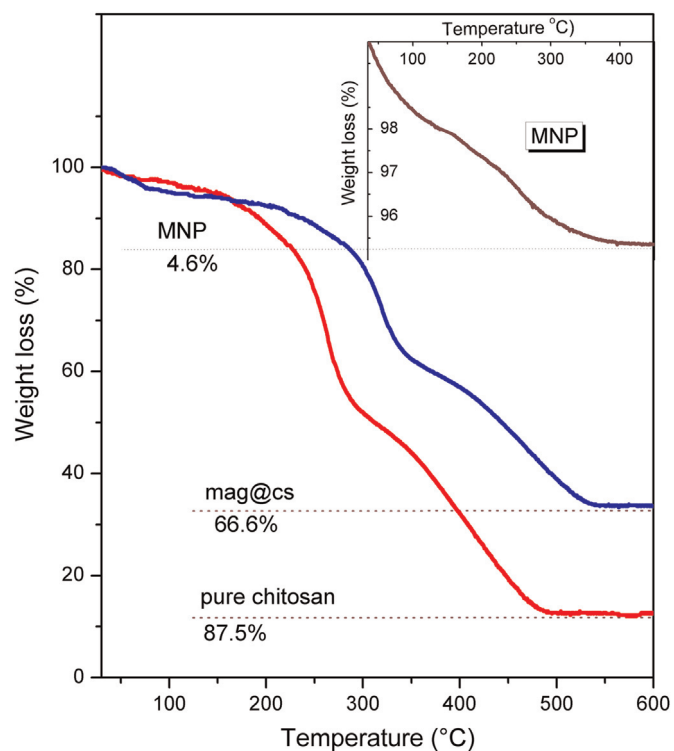


Fig. 5. Thermograms of mag@CS (blue) and pure chitosan (red) samples. The inset shows the weight loss observed in pure iron oxide nanoparticles. (For interpretation of the references to color in this figure legend, the reader is referred to the web version of this article.)

nanocomposite, which presents macroscopic features of magnetism as shown in inset (a) of Fig. 6. The room temperature magnetization curve for the mag@CS sample shown in this figure reveals that the synthesized composite presents a saturation magnetization of about 11.5 emu/g and that the magnetic properties of the composite originated mainly from MNPs, since chitosan

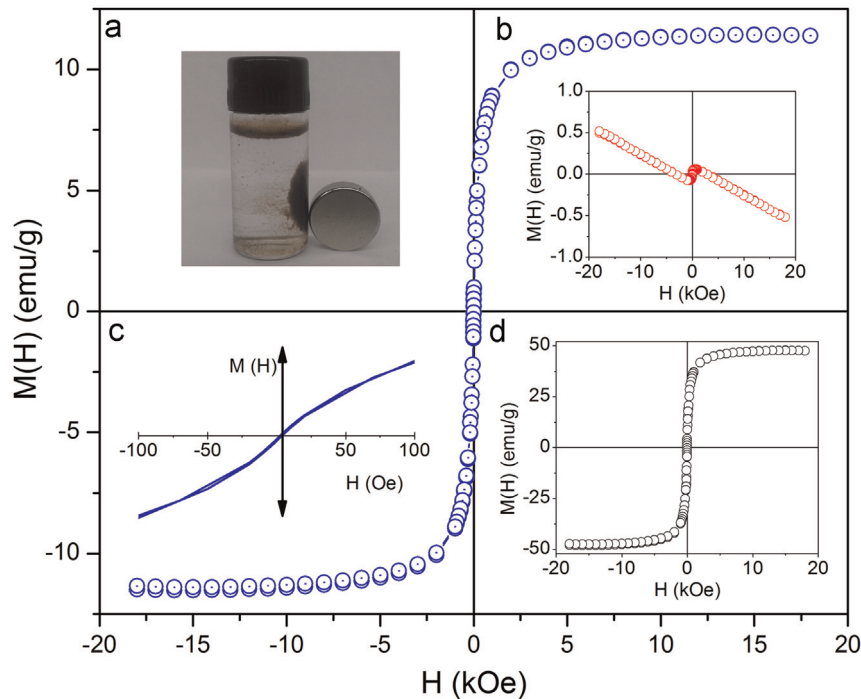


Fig. 6. Magnetization hysteresis loop at room temperature for sample mag@CS (blue circles). Picture of the magnetic chitosan under action of a permanent magnet (a), magnetization curve at room temperature of pure chitosan (b), magnetization data of mag@CS at low field range (c) and normalized only by the iron oxide mass (d). (For interpretation of the references to color in this figure legend, the reader is referred to the web version of this article.)

is a diamagnetic material, as presented in the magnetization curve of pure chitosan in inset (b). Moreover, MNPs displayed features of superparamagnetism such as negligible remanence and coercivity, observed in hysteresis loops – see inset (c), which shows the magnetization data at low field range.

Furthermore, if one normalizes magnetization only by the mass of the magnetic part, estimated from TGA analysis, saturation magnetization of the mag@CS sample is about 48 emu/g, typical of sub-10-nm sized magnetite/maghemite nanoparticles, as found by HRTEM measurements, probably due to cationic redistribution [23] and surface and size-finite effects that affect the magnetization characteristics of nanosized grains [24,25].

For samples loaded with 5-HTP, the quantity of amino acid incorporated in the composite structure was estimated by UV-vis analysis, comparing the spectra of supernatant with a calibration curve, after (dashed lines) and before (full lines) loading, as shown in Fig. 7. From this analysis, the mass percentage of 5-HTP incorporated on the composite when 5-HTP was added during synthesis (81.5%, w/w) was higher than 5-HTP loaded after magnetic composite synthesis (18.5%, w/w). This can be explained by the fact that, if it is added during synthesis, 5-HTP is embedded into the matrix by crosslinking within the polymeric structure or adsorbed onto the surface by chemical/physical interactions. In the case of 5-HTP incorporated after synthesis of mag@CS, surface adsorption is preponderant over embedding.

In order to investigate the effect of pH on the kinetics of drug release, the sample with 5-HTP incorporated during synthesis (i.e. with higher loading efficiency) was incubated in aqueous buffers at pH 3.5 and pH 8.5 at 25 °C. The curves of cumulative release as a function of time (Fig. 8) show that less than 7% and almost 90% of 5-HTP was released after 4 h of incubation, respectively, at pH 8.5 and pH 3.5. In both cases, the release rate is more important during the initial minutes and tends to stabilize as time advances. Here, drug release is higher in acidic media since solubility of CS increases as pH decreases, improving the diffusion of 5-HTP by

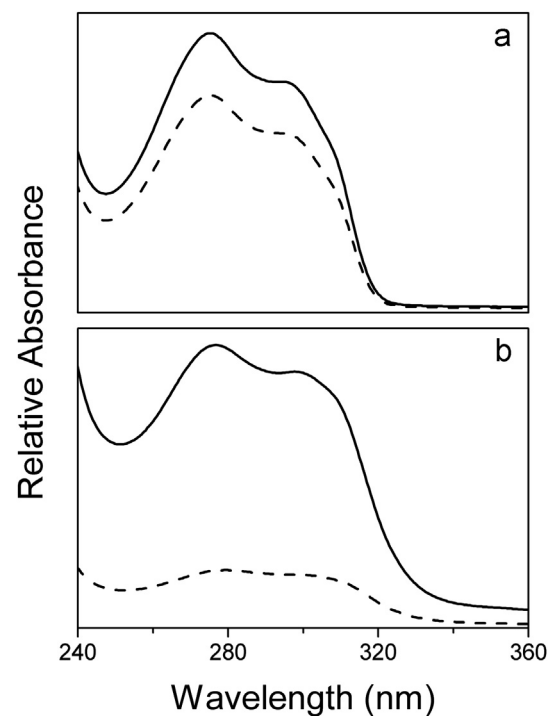


Fig. 7. UV-vis spectra of the supernatant before (full lines) and after (dashed lines) interaction of mag@CS with 5-HTP during the drug loading process. In (a) 5-HTP was loaded after magnetic composite synthesis and in (b) 5-HTP was added during synthesis.

erosion of polymer. At pH 8.5, chitosan is practically insoluble, so swelling seems to be the main mechanism of drug release.

Moreover, the Ritger and Peppas model [26] was applied to investigate the characteristics of drug release and confirms the previous qualitative observations. In this empirical model, the fraction of drug released (α) at a time t is proportional to kt^n where

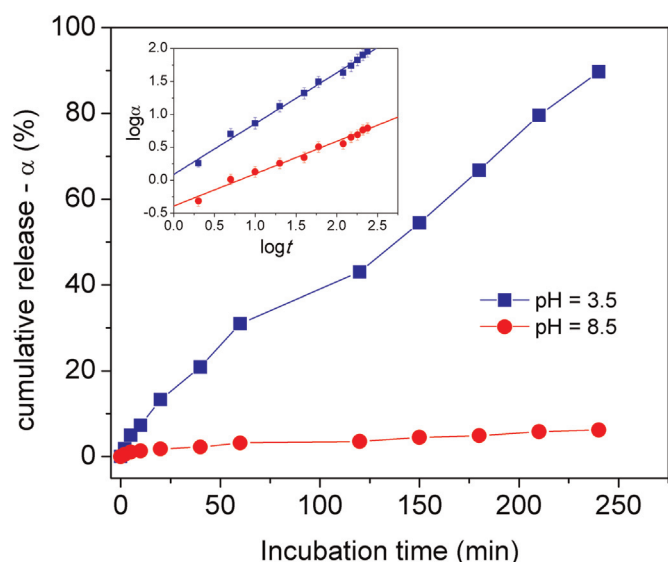


Fig. 8. Cumulative release of 5-HTP as a function of time for mag@CS samples at different pHs. The inset is a log–log plot and full lines are the linear fit of data.

Table 1

Drug release kinetic data obtained from fitting experimental data to the Ritger–Peppas equation.

pH	Maximal release (%)	Release rate constant (k)	Release exponent (n)	R^2
3.5	89.0	1.2	0.77	0.991
8.5	6.3	0.4	0.45	0.993

k is the release rate constant and n is the release exponent. The linear form of this equation (see the inset of Fig. 8) allowed, through its intercept and slope, the k and n parameters that are listed in Table 1 to be determined for the different experimental conditions. On the one hand, the difference in release rate constants as a function of incubation condition indicates that our nanocomposite is a pH-sensitive release system, and this rate is higher in an acidic medium.

On the other hand, according to the release exponents, at pH=8.5 drug transport slightly deviate from the Fickian model ($n=0.5$) of swelling-controlled release. At pH=3.5, the medium surrounding the nanocomposite may dissolve the polymer such as the rate that controls the drug release can be increased (i.e. dissolution competes with swelling) and anomalous drug transport is observed. Indeed, different n values and deviation from the Fickian diffusion model, that compare our results, were already observed for drug loaded chitosan and were related to the cross-linking degree [27] and drug loading concentration [28]. Moreover, the irregular shape and high polydispersity of samples can contribute to the variation of release characteristics [24].

4. Conclusions

Using homogeneous precipitation with urea, nanoparticles of chitosan in large aggregates, embedded with magnetic nanoparticles of magnetite/maghemite of ~ 7 nm and narrow size-distribution could be synthesized. One of the advantages of this procedure was that a selected drug (5-HTP) could be efficiently incorporated during the synthesis of the nanomaterial in a simple and one-step procedure. The release of 5-HTP has been shown time and pH-dependent and seems to be modulated by diffusion arising from swelling and/or dissolution of polymer. Due to the chemical nature

of the components of composite (chitosan and iron oxides) drug loading could be extended to a series of drugs different of 5-HTP and, owing to its magnetization features, composite could be easily manipulated by an external magnetic field to be delivered and/or concentrated in a determined region, improving the efficiency of the release purposes. Moreover, decomposition/swelling of chitosan is temperature dependent so that thermal heating (magneto hyperthermia) could be utilized to better control drug release. In this way, the synthesis route presented here has great potential as high efficiency, cost effective and environment-friendly materials for the elaboration of stimuli-responsive materials for applications in the field of controlled drug-release systems. Future work will include the minimization of the aggregate size and its dispersion in a colloidal matrix that enables its use for controlled drug release.

Acknowledgement

The authors gratefully acknowledge financial support from the Conselho Nacional de Desenvolvimento Científico e Tecnológico (CNPq (Grant no. 564180/2010-6)), Fundação de Apoio à Pesquisa do Distrito Federal (FAPDF (Grant no. 193.000.480/2011)) and Fundação de Empreendimentos Científicos e Tecnológicos (Finatec).

References

- [1] P.H.L. Tran, T.T.D. Tran, J.B. Park, B.J. Lee, Controlled release systems containing solid dispersions: strategies and mechanisms, *Pharm. Res.-Dordr.* 28 (2011) 2353–2378.
- [2] K.S. Soppimath, T.M. Aminabhavi, A.R. Kulkarni, W.E. Rudzinski, Biodegradable polymeric nanoparticles as drug delivery devices, *J. Control Release* 70 (2001) 1–20.
- [3] S.A. Agnihotri, N.N. Mallikarjuna, T.M. Aminabhavi, Recent advances on chitosan-based micro- and nanoparticles in drug delivery, *J. Control Release* 100 (2004) 5–28.
- [4] J.O. You, D. Almeida, G.J.C. Ye, D.T. Auguste, Bioresponsive matrices in drug delivery, *J. Biomed. Eng.* 4 (2010) 15. <http://dx.doi.org/10.1186/1754-1611-4-15>.
- [5] Q.A. Pankhurst, N.T.K. Thanh, S.K. Jones, J. Dobson, Progress in applications of magnetic nanoparticles in biomedicine, *J. Phys. D: Appl. Phys.* 42 (2009) 224001–224015.
- [6] P. Tartaj, M.P. Morales, S. Veintemillas-Verdaguer, T. González-Carreño, C. J. Serna, The preparation of magnetic nanoparticles for applications in biomedicine, *J. Phys. D Appl. Phys.* 36 (2003) R182–R197.
- [7] L.H. Reddy, J.L. Arias, J. Nicolas, P. Couvreur, Magnetic nanoparticles: design and characterization, toxicity and biocompatibility, pharmaceutical and biomedical applications, *Chem. Rev.* 112 (2012) 5818–5878.
- [8] D.H.K. Reddy, S.M. Lee, Application of magnetic chitosan composites for the removal of toxic metal and dyes from aqueous solutions, *Adv. Colloid Interface* 201 (2013) 68–93.
- [9] T.S. Anirudhan, S.S. Gopal, S. Sandeep, Synthesis and characterization of montmorillonite/N-(carboxyacyl) chitosan coated magnetic particle nanocomposites for controlled delivery of paracetamol, *Appl. Clay Sci.* 88–89 (2014) 151–158.
- [10] K.H. Bae, M. Park, M.J. Do, N. Lee, J.H. Ryu, G.W. Kim, C. Kim, T.G. Park, T. Hyeon, Chitosan oligosaccharide-stabilized ferrimagnetic iron oxide nanocubes for magnetically modulated cancer hyperthermia, *ACS Nano* 6 (2012) 5266–5273.
- [11] A.P.N. Majumdar, Tryptophan requirement for protein-synthesis – a review, *Nutr. Rep. Int.* 26 (1982) 509–522.
- [12] L. Gordon, M.L. Salutsky, H.H. Willard, *Precipitation from Homogeneous Solution*, Wiley, New York, 1959.
- [13] K. Kaibara, T. Okazaki, H.B. Bohidar, P.L. Dubin, pH-induced coacervation in complexes of bovine serum albumin and cationic polyelectrolytes, *Biomacromolecules* 1 (2000) 100–107.
- [14] A.L. Drummond, N.C. Feitoza, G.C. Duarte, M.J.A. Sales, L.P. Silva, J.A. Chaker, A. F. Bakuzis, M.H. Sousa, Reducing size-dispersion in one-pot aqueous synthesis of maghemite nanoparticles, *J. Nanosci. Nanotechnol.* 12 (2012) 8061–8066.
- [15] M.A. Morales, E.C.D. Rodrigues, A.S.C.M. de Amorim, J.M. Soares, F. Galembeck, Size selected synthesis of magnetite nanoparticles in chitosan matrix, *Appl. Surf. Sci.* 275 (2013) 71–74.
- [16] J.C. Rubim, M.H. Sousa, J.C.O. Silva, F.A. Tourinho, Raman spectroscopy as a powerful technique in the characterization of ferrofluids, *Braz. J. Phys.* 31 (2001) 402–408.
- [17] H.Y. Huang, Y.T. Shieh, C.M. Shih, Y.K. Twu, Magnetic chitosan/iron (II, III) oxide nanoparticles prepared by spray-drying, *Carbohydr. Polym.* 81 (2010) 906–910.

- [18] K.M. Gregorio-Jáuregui, M.G. Pineda, J.E. Rivera-Salinas, G. Hurtado, H. Saade, J. L. Martínez, A. Ilyina, R.G. López, One-step method for preparation of magnetic nanoparticles coated with chitosan, *J. Nanomater.* (2012).
- [19] N.C. Feitoza, T.D. Gonçalves, J.J. Mesquita, J.S. Menegucci, M.K.M.S. Santos, J. A. Chaker, R.B. Cunha, A.M.M. Medeiros, J.C. Rubim, M.H. Sousa, Fabrication of glycine-functionalized maghemite nanoparticles for magnetic removal of copper from wastewater, *J. Hazard. Mater.* 264 (2014) 153–160.
- [20] T. Sannan, K. Kurita, Y. Iwakura, *Studies on Chitin. 2. Effect of deacetylation on solubility*, *Makromol. Chem.* 177 (1976) 3589–3600.
- [21] G.A.F. Roberts, *Chitin Chemistry*, MacMillan, London, 1992.
- [22] Y.L. Wang, B.Q. Li, Y. Zhou, D.C. Jia, In situ mineralization of magnetite nanoparticles in chitosan hydrogel, *Nanoscale Res. Lett.* 4 (2009) 1041–1046.
- [23] J.A. Gomes, M.H. Sousa, F.A. Tourinho, J. Mestnik, R. Itri, J. Depeyrot, Rietveld structure refinement of the cation distribution in ferrite fine particles studied by X-ray powder diffraction, *J. Magn. Magn. Mater.* 289 (2005) 184–187.
- [24] E.C. Sousa, M.H. Sousa, G.F. Goya, H.R. Rechenberg, M.C.F.L. Lara, F.A. Tourinho, J. Depeyrot, Enhanced surface anisotropy evidenced by Mossbauer spectroscopy in nickel ferrite nanoparticles, *J. Magn. Magn. Mater.* 272 (2004) E1215–E1217.
- [25] J.F. Saenger, K.S. Neto, P.C. Morais, M.H. Sousa, F.A. Tourinho, Investigation of the anisotropy in frozen nickel ferrite ionic magnetic fluid using magnetic resonance, *J. Magn. Reson.* 134 (1998) 180–183.
- [26] N.A. Peppas, J.J. Sahlin, A simple equation for the description of solute release. 3. Coupling of diffusion and relaxation, *Int. J. Pharm.* 57 (1989) 169–172.
- [27] S.A. Agnihotri, T.M. Aminabhavi, Controlled release of clozapine through chitosan microparticles prepared by a novel method, *J. Control Release* 96 (2004) 245–259.
- [28] S.G. Kumbar, A.R. Kulkarni, T.M. Aminabhavi, Crosslinked chitosan microspheres for encapsulation of diclofenac sodium: effect of cross-linking agent, *J. Microencapsul.* 19 (2002) 173–180.